Harnessing the Wharton's jelly membrane osteo-biocompatibility by a tannic acid cross-linking

Loïc Scomazzon, F Lemaire, Marie Dubus, J Braux, Christine Terryn, A Baldit, J.S. Lecomte, Quentin Carboué, C Guillaume, N Bouland, et al.

Applied Materials Today 39 (2024) 102241

Contents lists available at ScienceDirect

Applied Materials Today

journal homepage: www.elsevier.com/locate/apmt

Harnessing the Wharton's jelly membrane osteo-biocompatibility by a tannic acid cross-linking

L. Scomazzon [a], F. Lemaire [a], M. Dubus [a], J. Braux [a,b], C. Terryn [c], A. Baldit [d], J.S. Lecomte [d], Q. Carboué [e], C. Guillaume [a], N. Bouland [a], E. Brenet [a,f], F. Boulmedais [g], C. Mauprivez [a,b], H. Kerdjoudj [a,*]

[a] University of Reims Champagne Ardenne, Reims, France
[b] Pôle de santé buccodentaire, CHU de Reims, Reims, France
[c] University of Reims Champagne Ardenne, PICT platform, Reims, France
[d] University of Lorraine, CNRS UMR 7239 LEM3, Metz, France
[e] URD Agro-Biotechnologies Industrielles (ABI), CEBB, AgroParisTech, Pomacle, France
[f] Pôle tête et cou, Oto rhino laryngologie, CHU de Reims, Reims, France
[g] University of Strasbourg, CNRS Institut Charles Sadron, Strasbourg France

ARTICLE INFO

Keywords:
Wharton's jelly
Polyphenols
Antioxidant
Antibacterial
Bone regeneration

ABSTRACT

Decellularized extracellular matrix is a promising material for regenerative medicine applications. Decellularized Wharton's jelly (WJ) is considered as a favorable allograft based material due to its biological properties including antibacterial activities, and immunomodulation. However, the rapid degradation and poor mechanical behavior of WJ derived membranes in biological environment hinders their application in guided bone regeneration. In this study, we have demonstrated that tannic acid (TA), a natural polyphenol, is an efficient cross-linking agent to significantly improve the mechanical properties and the enzymatic stability of WJ membranes. In addition, the post-oxidation of WJ-TA membranes, by sodium periodate, endowed superior biological properties. Indeed, WJ-TA oxidized (WJ-TA-ox) membranes showed antibacterial and antioxidant activities along with a better performance *in vitro*, improving primary osteoblast and dental pulp stromal cell adhesion and proliferation, and *in vivo*, increasing the *de novo* bone formation in a parietal bone defect. These results showed the osteo-biocompatibility and the great potentials of WJ-TA-ox membranes for bone regenerative medicine.

1. Introduction

A major challenge in regenerative medicine is to accurately reproduce the biochemical, physical and mechanical environment of a native extracellular matrix (ECM). The unique ultrastructure of the ECM induces tissue repair while does not stimulating a negative immune response of the host, thereby enhancing the success rate after implantation [1]. Scaffolds produced from decellularized ECM provide a unique spatial distribution of structural and bioactive components that trigger the innate healing and regenerative processes [2]. The process of decellularization aims to remove cells and immunogenic molecules while preserving structural proteins [3]. Urinary bladder and small intestinal submucosa are common bioactive decellularized biomaterials approved by the Food and Drug Administration (FDA) with proven outcomes in skin, muscle, and gastrointestinal tissue damages [4]. Since May 2020, the European Union's new regulation considered human tissues or derivatives as a high-risk medical devices (class III).

Human perinatal tissues, birth-associated tissues such as the placenta and its annexes are recovered from healthy individuals and discarded at the birth without ethical constraints, providing ample opportunity for harvesting compared to cadaveric allograft donation. Perinatal tissues provide an inexhaustible source of ECM components and cells for the field of regenerative medicine [5,6]. Wharton's jelly (WJ), a part of the umbilical cord, is a rich reservoir of mesenchymal stromal cells, growth factors, and contains significant amounts of collagen, hyaluronic acid, and glycosaminoglycans. A combination of detergent and enzymes has been successfully used to efficiently decellularize WJ matrix, increasing the release of angiogenic vascular endothelial growth factors and macromolecules with antibacterial and immunomodulatory properties [7,8]. Recent studies have used decellularized perinatal tissues to produce

* Corresponding author at: Université de Reims Champagne Ardenne, 1 avenue du Maréchal Juin, 51100 Reims, France.
E-mail address: halima.kerdjoudj@univ-reims.fr (H. Kerdjoudj).

https://doi.org/10.1016/j.apmt.2024.102241
Received 15 January 2024; Received in revised form 26 April 2024; Accepted 13 May 2024
Available online 31 May 2024

biomaterials from micronized particles followed by reconstitution them into various forms of biomaterials such as hydrogel [9-11], membrane [12-14], sponge, [15] and electrospun scaffolds [16,17]. Although perinatal tissues have already been used for wound healing and the treatment of surface defects in ophthalmology [18], few clinical studies have assessed their potential as a scaffold in orthopedic and craniofacial applications [19,20].

The biodegradability and controlled degradation rate are highly beneficial for bone substitutes. Despite the above attractive properties of the WJ matrix, its high degradation rate *in vivo* limits its widespread use in hard tissue [7]. The application of the FDA-approved tannic acid (TA) in biomedicine has received extensive attention in these recent years [21,22]. Composed of a complex mixture of highly reactive phenolic hydroxyl groups, the TA provides both biological stability and high cross-linking potential for collagen. The phenolic hydroxyl groups of TA can form hydrogen bonds with the carbonyl and amino group of collagen [23]. Under acidic conditions favorable for hydrogen bonding, TA in its non-oxidized form provides a weak cross-linking ability of collagen compared to its oxidized form [24]. In fact, the oxidation of TA converts the phenols into a quinone-rich structure that can covalently react with the amino groups of the collagen through Schiff base reaction and Michael addition reaction [25]. In addition to the cross-link capabilities, TA also exhibits a wide range of restorative, therapeutic and pharmacological properties including anticancer, antioxidant, anti-inflammatory, antimicrobial, wound healing, and homeostatic [21].

Although previous studies have demonstrated the high potential of decellularized WJ membrane for soft tissue regeneration [7,8], no studies have evaluated the effect of applying multifunctional WJ-TA membrane for the bone regeneration defects. In this study, we aimed to develop a multifunctional membrane composed of WJ and TA to alleviate the bone regeneration failure after implantation. Herein, decellularized WJ (*i.e.* mainly composed mainly of collagen [8]) was cross-linked with TA in a non-oxidized (WJ-TA) and oxidized (WJ-TA-ox) form, aiming to improve its osteobiocompatibility (*i.e.* mechanical, thermal, and biological performances). The WJ-TA-ox multifunctional membrane allowed the regeneration of parietal bone defects and may serve as a promising scaffold for future clinical treatment.

2. Materiel and methods

All human samples were obtained from informed patients (written consent) and in compliance with the Bioethic law (article R 1243–47). All further samples handling procedures were performed within the frame of our specific authorization and registration number DC-2014–2262 issued by the National French "*Cellule de Bioéthique*". All reagents came from (Sigma-Aldrich, France) unless specified.

2.1. Samples preparation

Wharton's Jelly membranes (WJ) were obtained after the removal of the amniotic membrane and blood vessels and decellularization as previously described [8]. Freeze-dried WJ (250 mg) were incubated in TA (750 mM) /citrate buffer (0.1 M, pH = 4) under rotary shaking for 24 h and at 37 °C in the dark. The resulting Wharton's Jelly-tannic acid (WJ-TA) membrane was then oxidized using sodium metaperiodate ($NaIO_4$, 23 mM) for 2 h at 37 °C in the dark. WJ-TA and oxidized WJ-TA-(ox) membranes were rinsed for 48 h in phosphate buffered saline (PBS, Gibco, France), freeze-dried and stored at – 20 °C until use.

2.2. Membranes characterizations

2.2.1. Fourier transform infrared spectroscopy

Freeze-dried WJ-TA and WJ-TA-ox membranes were analyzed using a Vertex 70 spectrometer (Bruker, Germany) using a DTGS detector. Spectra were recorded in the Attenuated Total Reflection (ATR) mode using single reflection diamond ATR, averaging 128 interferograms between 1100 and 1800 cm^{-1} at 2 cm^{-1} resolution and using Blackman-Harris three-term apodization and Bruker OPUS/IR software (version 7.5).

2.2.2. Hematoxylin-Eosin-Saffron (HES) staining

Freeze-dried WJ-TA and WJ-TA-ox membranes were embedded in paraffin, cut (5 μm thick sections) using a rotary microtome HM340E (MM France) and stained before further examination using an OLYMPUS VS 120 scanner (Shinjuku-ku, Japan).

2.2.3. Scanning electron microscopy

Freeze-dried WJ-TA and WJ-TA-ox membranes were sputtered with a thin film of gold-palladium (Ion sputtering JEOL JFC 1100, France) and observed at SEM evo 10 (Zeiss, Germany).

2.2.4. Ninhydrin assay

Crosslinking degree was evaluated by determination of free amine groups present on WJ-TA and WJ-TA-ox membranes. WJ membrane was used as control. Ninhydrin (200 mg) and hydrindantin (30 mg) were dissolved in dimethyl sulfoxide (DMSO, 7.5 mL) and acetate buffer (0.1 M, pH 5.2) was added to obtain a final volume of 10 mL (reaction solution). Each freeze-dried sample (1 mg) was mixed with reaction solution (100 μL) and incubated for 10 min at 100 °C in a dry bath. Stabilization solution (ethanol 50°) was added, vortexed and each supernatant sample (200 μL) were deposited in duplicate to a 96-well plate. The absorbance (A) was read at 575 nm and corrected at 750 nm, using a FLUOstar Omega microplate reader (BMG Labtech, France). The Crosslinking degree was obtained as follow:

$$\text{Cross}-\text{linking degree} = \left(\frac{\left(A_{\text{sample}} - A_{\text{blanck}}\right) - \left(A_{\text{WJ}} - A_{\text{blanck}}\right)}{A_{\text{WJ}} - A_{\text{blanck}}}\right) \times 100$$

2.2.5. Liquid displacement

The moister content (MC) and gravimetric swelling (GS) were determined by a sample's absorption of PBS. WJ-TA, WJ-TA-ox and WJ membranes (10 mg) were immersed in PBS for 15 min and the wet weight (W) was measured. MC and GS were calculated using the following equations:

$$\text{MC}\ (\%) = \left(\frac{W - 10}{W}\right) \times 100$$

$$\text{GS}\ (\%) = \left(\frac{W - 10}{10}\right) \times 100$$

2.2.6. Total matrices porosity

Freeze-dried WJ-TA, WJ-TA-ox and WJ membranes (10 mg) were immersed in absolute ethanol for 15 min and samples were weighted. The pore volume occupied ethanol was determined by the following equation:

$$\text{Porosity}\ (\%) = \left(\frac{W - 10}{W}\right) \times 100$$

2.2.7. Contact angle measurement

Contact angle measurement was performed on WJ-TA, WJ-TA-ox and WJ membranes at room temperature with a drop shape analyzer - DSA25 (Kruss-scientific, Germany) following the deposit of demineralized water (1.5 μL) on the membrane' surface.

2.2.8. Released tannic acid

Released TA from the freeze-dried WJ-TA and WJ-TA-ox membranes was evaluated over a period of 52 h. Each freeze-dried sample (5 mg) was incubated at 37 °C in PBS (1 mL) and the released TA from each sample' supernatant was measured at $l_{280\ nm}$ using a Nanodrop®

(Thermo Fisher Scientific, United States). The results are expressed in "mg" by comparison with a TA standard curve.

2.2.9. In vitro antioxidant activity

The antioxidant activity of the freeze-dried WJ-TA and WJ-TA-ox membranes was monitored using the free radical scavenging test 2,2-diphenyl-1-picrylhydrazyl (DPPH•). WJ membrane was used as a control. Each sample (10 mg) was incubated in PBS at 37 °C for 2 h. Sample's supernatants were mixed with a solution of DDPH• diluted in methanol (0.04 mg/mL). Blank corresponds to a mixture of PBS with DDPH•. Samples were deposited into a 96-well plate, incubated for 5 min at room temperature and $A_{515\ nm}$ was determined using an Epoch 2 microplate reader (BioTeck, USA). The radical scavenging activity (% inhibition) was assessed as following:

$$\text{Inhibition } (\%) = \left(\frac{A_{blank} - A_{samples}}{A_{blanck}}\right) \times 100$$

2.2.10. Mechanical properties

Mechanical properties of samples were evaluated by quasi-static tensile tests until failure using a Zwicky Universal Testing Machine (ZwickRoell, Germany) equipped with a 10 N load cell. The loading sequence was divided into two stages: a dry test under the linear elastic limits with an imposed deformation around 1.6% to avoid any damage, followed by a hydrated test (NaCl 0.9%, 37 °C) allowing a complete characterization of the mechanical response up to failure [7,8,26]. Between the two steps, the sample was given 5 min to hydrate and reach osmotic balance before being tested. All loadings were performed at a speed of 0.01 mm/s to stay within the quasi-static frame. The engineer definition of stress and strain was used to process the force displacement curves and measure the elastic moduli.

2.2.11. In vitro degradation

Freeze-dried WJ-TA, WJ-TA-ox and WJ membranes (10 mg) were immersed in collagenase type II or in porcine pepsin/ HCl 0.1 M (1 mg/mL, Gibco, France) for 72 h at 37 °C. The undigested samples were freeze-dried and weighted. The percentage of remaining mass was determined as following:

$$\text{Degradation } (\%) = \left(\frac{10}{W}\right) \times 100$$

2.2.12. Thermogravimetric analysis

Freeze-dried WJ-TA, WJ-TA-ox and WJ membranes were heated from room temperature to 500 °C at a heating rate of 5 °C/min under nitrogen atmosphere by maintaining a nitrogen flow rate of 20 mL/min using Thermogravimetric Analyser Q500. The first derivative of the TGA curve (DTG curve) was determined as following to determine inflection points (m_i = *initial mass (%)* ; t_i = *intial temperature (°C)*):

$$DTG = \frac{m_i - m_{i-1}}{t_i - t_{i-1}}$$

2.2.13. Antibacterial properties

Staphylococcus aureus (*S. aureus*) strain SH1000 preculture were incubated overnight in Mueller-Hinton broth (Biokar diagnostics, France) at 37 °C. For all experiments, the absorbance of *S. aureus* overnight culture was measured at 600 nm and was adjusted to 0.2 (~10^8 CFU/mL). Under sterile conditions, 5 µL were diluted in 1 mL of physiologic water in 24-well plates in the presence of UV-decontaminated freeze-dried WJ-TA, WJ-TA-ox or WJ membranes (1 cm^2) and incubated at 37 °C. After 1, 2, 4 and 24 h, serial dilutions were performed and 100 µL dilutions were plated on TSA exponentially with the easySpiral Pro (Interscience, France). After 24 h of incubation at 37 °C, the colony forming units on the agar plates were counted with the Scan 1200 (Interscience, France).

2.3. Biocompatibility

2.3.1. Ames test

The mutagenic potential of WJ-TA and WJ-TA-ox membranes was assessed using the *Salmonella typhimurium* TA1000 (Trinova Biochem, Germany) for the Ames test [27]. Briefly, TA1000 precultures were incubated in oxoid Nutriment Broth #2 at 37 °C for 24 h. Freeze-dried WJ-TA, WJ-TA-ox and WJ membranes (1 cm^2) were UV-decontaminated for 20 min and incubated in PBS at 37 °C for 24 h. The absorbance of the TA1000 preculture was measured at 620 nm and was adjusted to 0.5. Then, sample's extracts (500 µL) were incubated for 20 min at 37 °C with PBS (100 µL), distilled water (200 µL), histidine/biotin (0.5 M, 100 µL) and TA1000 preculture (100 µL). TA1000 preculture in PBS and NaN_3 (3 µg/mL) were used as negative and positive mutagenic controls, respectively. All the experimental conditions were placed on Minimal Glucose Agar Plates and incubated for 48 h at 37 °C before counting the bacterial colonies.

2.3.2. Cell culture

Human dental pulp stromal cells (DPSCs) isolated from the dental pulp of 3rd molars, gingiva fibroblasts and mandibular osteoblasts were obtained as previously described [7]. DPSCs were grown in α-MEM culture medium (LONZA, France) supplemented with Glutamax® (1%, *v/v*), Penicillin/Streptomycin/Amphotericin cocktail (PSA, 1%, *v/v*) and decomplemented fetal bovine serum (FBS) for 30 min at 56 °C (10%, *v/v*). Fibroblasts and osteoblasts were cultured in DMEM-Glutamax® culture medium supplemented with PSA (1%, *v/v*) and decomplemented FBS (10%, *v/v*).

2.3.3. Intracellular reactive oxygen species (ROS)

Fibroblasts were seeded at 10^4 cells/cm^2 in six-well plates and cultured at 37 °C, 5% CO_2 until reaching 70–80% of confluence. UV-decontaminated freeze-dried WJ-TA, WJ-TA-ox and WJ membranes (1 mg) were then added and incubated for 24 h. Hydrogen peroxide (1 mM) was added, incubated for 3 h and cells were harvested following the trypsin-EDTA treatment. The intracellular ROS was labeled according to the manufacturer instructions (Muse® Oxidative Stress Kit, Luminex) and analyzed by flow cytometry acquisition with a LSRFortessa™ system (BD Biosciences, France).

2.3.4. Viability assay

DPSCs, gingiva-derived fibroblasts and osteoblasts were seeded at 2.4 x 10^4 cells/cm^2 and cultured until reaching 70–80 % of confluence. UV-decontaminated freeze-dried WJ-TA, WJ-TA-ox and WJ membranes (1 mg) were added to cells and cultured for 24 h. Cells cultured without samples were used as controls. The cells metabolic activity measurement was carried out by a water-soluble tetrazolium salt (WST-1®) assay in accordance with the manufacturer's protocol. The A was measured at 440 nm with a correction at 750 nm, using a FLUOstar Omega microplate reader.

2.3.5. Cell proliferation assay and cell visualization

DPSCs, gingiva-derived fibroblasts, and osteoblasts were seeded at 2.4 x 10^4 cells/cm^2 on UV-decontaminated WJ-TA, WJ-TA-ox and WJ membranes. For that, membranes were glued to the culture plate well and after 3, 7 and 14 days of culture, membranes were peeled off and the cell metabolic activity of adhered cells was assessed by WST-1® assay. After 14 days of culture, adhered cells were fixed with paraformaldehyde (4%, *w/v,* Sigma-Aldrich, Germany) at 37 °C for 10 min, permeabilized with Triton 100-X (0.5%, *v/v*) for 5 min and incubated in Alexa® Fluor-488 conjugated-Phalloidin® (1/100 dilution in 0.1% Triton 100-X) for 45 min at room temperature. Nuclei were counterstained with 4,6-diamidino-2- phenylindole (DAPI, 100 ng/mL, 1/10 000 dilution) for 5 min. Labelled cells were mounted and imaged by confocal laser scanning microscopy CLSM, 710 NLO, 20× objective, numerical aperture 0.8 (Zeiss, Germany). After 14 days of culture,

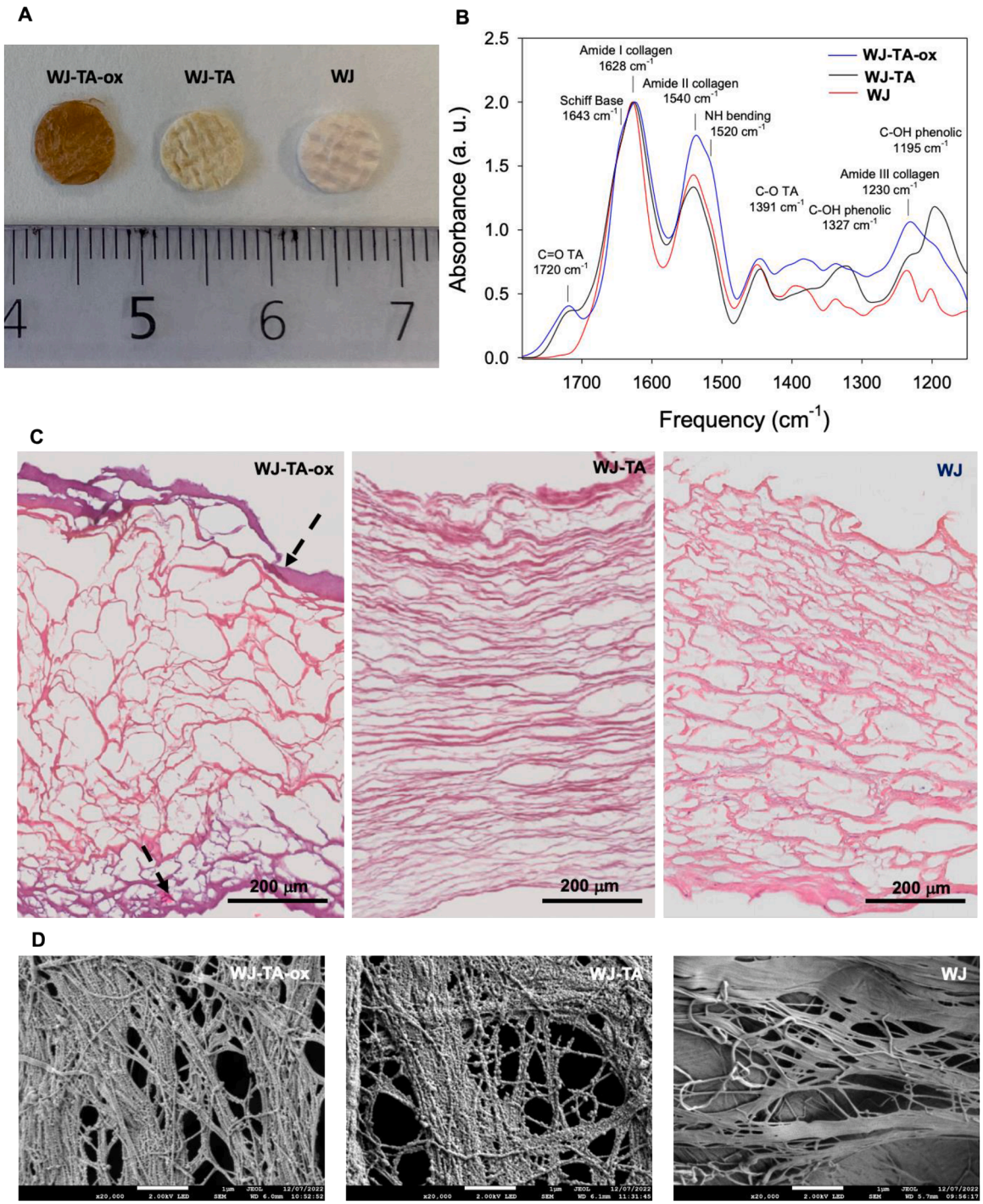

Fig. 1. Morphological evaluation of the tannic acid cross-linked Wharton's jelly membranes. A: Macroscopical views, showing changes in WJ color after processing. B: FTIR spectra of the three WJ membranes. C: Histological section and HES staining of the three WJ membranes, indicated porous membranes with a limited $NaIO_4$ reaction at the membrane borders (dashed black arrows; scale bars = 200 µm). D: SEM images, highlighting pearl necklace-like structure of the collagen fibers in the presence of TA (scale bars = 1 µm). TA-ox = oxidized tannic acid, TA = tannic acid, and WJ = Wharton's jelly membranes.

adhered cells were fixed in formalin at room temperature for a week, dehydrated and embedded in paraffin. Sections of 4 µm-thick, using rotary microtome RM2055, were stained (HES staining) and images using VS.120 scanner.

2.3.6. *In vivo performance*

Animal experiments were carried out in accordance with the 3R rule and following the approval of the animal protection commission of the University of Reims Champagne-Ardenne for a subcutaneous implantation model (#33,870- 2,021,111,219,002,699) and for a parietal bone defect model (#33,853–2,021,101,512,003,812). All animals were anesthetized by inhalation of 2.5% isoflurane (isuflu-vet, Netherland) and euthanized at the end of each procedure by cervical dislocation preceded by over-inhalation of 5% isoflurane.

2.3.7. *Subcutaneous implantation*

Host's response to the UV-decontaminated WJ-TA, WJ-TA-ox and WJ membranes was assessed with immunocompetent eight-week-old

male Wistar rats ($n = 4$). Each sample (10 mg) was implanted subcutaneously in rat and left for seven weeks. Explanted samples were fixed in formalin, dehydrated, and then embedded in paraffin. Histological sections (6 μm-thick) were stained HES and Masson's trichrome (MT) then scanned using an OLYMPUS VS 120 scanner.

2.3.8. Parietal bone defect

Parietal bone defect was performed on immunocompetent eight-week-old male Wistar rats ($n = 11$) as published elsewhere [28]. Right and left parietal bone defects were respectively covered with UV-decontaminated WJ-TA and WJ-TA-ox membranes (6 mm diameter), then, the periosteum and skin were carefully sutured. At two and four weeks post-surgery, *in vivo* imaging using micro-computed tomography (m-CT, scans Skyscan 1076, Bruker, Belgium) with the following settings: tube voltage, 80 kV; tube current, 0.125 mA; and 35.8 μm^3 voxel size was performed. At eight weeks, animals were sacrificed and parietal bone was collected and immediately fixed in formalin for a week then stored in 70% ethanol and imaged with m-CT with the following settings: tube voltage, 70 kV and 17.9 μm^3 voxel size. Three-dimensional (3D) images were reconstructed, reoriented and analyzed using the NRecon GPU version, Dataviewer and CTAn 1.18 software. After 3D reconstruction, bone volumes were segmented using a global threshold obtained by using the mean value of densities leading to segment bone, and only bone, outside of the treated region, retrieved in each scan after manual segmentation. Bone volume/total volume ratio (BV/TV) were measured in a region of interest consisting of a cylinder of 6 mm diameter and 2.5 mm height and manually centered into the defect. Views presented in the coronal and transaxial plane were obtained using an open-source image processing software (ImageJ version 2.9). The formalin-fixed explanted parietal bone ($n = 3$) was dehydrated in ethanol baths, embedded in resin (Technovit® 9100, Germany), sliced at a 6 μm thickness and stained with MT.

2.3.9. Nanoindentation

The central portions of the left and right parietal bone defect ($n = 8$) were dehydrated in a series of ascending ethanol baths before being embedded vertically in epoxy resin (SOLO Past vosschemie, France) and placed under vacuum to allow the epoxy to fill all spaces. Using a low-speed saw (ISOMETTM Low-Speed Saw, Bühler, USA) and a diamond blade, the test surface, the width of the bone, was exposed and then polished to using series of descending diamond suspension pastes (9 μm, 3 μm, 1.5 μm and 0.05 μm) with polishing cloths on a polishing machine (MetaServ® 250 Grinder-Polisher with Vector® LC Power Head, Bühler, USA). Samples were washed in deionized water using an ultrasonic bath to avoid cross-contamination between suspension pastes. Nanoindentation was performed on a NanoIndenter UNHT^3 (Anton Paar, Austria) with load and displacement resolutions of 50 nN and < 0.01 nm respectively. A Berkovich diamond indentation tip with a modulus of elasticity of 1141 GPa and a Poisson's ratio of 0.07 was used. Machine calibration was performed using fused silica. 10 imprints were made on each sample, the imprints being at least 10 μm from the edge of the sample and 15 μm from the neighbor. The loading profile included two conditioning stages that reached ¼ max load and ½ max load, followed by a third stage that reached a max load of 20 mN. Multiple loading cycles, as well as a long wait of 120 s at each peak load, reduce the impacts of time-dependent mechanical response.

2.3.10. Statistical analysis

All statistical analyzes were performed with the GraphPad Prism 9.5.0. The structural and physicochemical properties were evaluated with a minimum of four samples per condition. The cytocompatibility, intracellular ROS and cellular behavior on the samples was evaluated with four independent donors of DPSCs, fibroblasts and osteoblasts and all freeze-dried samples were tested in triplicate. Ames test was performed on three independent bacterial precultures. *In vivo* experiments were performed on 15 rats. Micro-CT was performed on all rats and nanoindentation experiment on eight explanted parietal bones. Results were presented with boxplots and histograms (mean ± SEM). Statistical analyzes were performed using ANOVA and Mann & Whitney test. For each test, a value of $p < 0.05$ was accepted as statistically significant p (level of rejection of the null hypothesis of equality of means).

Table 1
Physicochemical characteristics of the tannic acid-cross-linked Wharton's jelly membranes.

	WJ-TA-ox	WJ-TA	WJ	p
Crosslink degree (%)	59 ± 9*	27 ± 7	–	* $p < 0.0001$
Gravimetric swelling (%)	679 ± 248$	1033 ± 389$	2259 ± 780	$ $p < 0.002$
Moisture content (%)	86 ± 5$	90 ± 3$	95 ± 2	$ $p < 0.002$
Total porosity (%)	81 ± 4$	82 ± 3$	93 ± 1	$ $p < 0.002$
Wettability (°)	51 ± 4*	57 ± 5$	45 ± 2	* $p < 0.003$, $ $p < 0.0003$

* *vs.* WJ-TA, ($) *vs.* WJ, ANOVA statistical test.

3. Results and discussion

After decellularization, WJ membranes, consisting mainly of collagen [8], were cross-linked with tannic acid (TA) to form WJ-TA membrane. TA was used at a low concentration (0.125%), avoiding its polymerization and the formation of aggregates [24,29]. Sodium periodate ($NaIO_4$) can oxidize phenols and convert them into a quinone-rich structure which may react with histidine, lysine and cysteine and form covalent cross-link [25]. Post-oxidation of WJ-TA membranes was performed using a molar excess of $NaIO_4$ (0.5%) [25] to obtain WJ-TA-ox membranes. After decellularization, WJ membranes appear white [8]. A color change of the WJ membranes was observed after TA cross-linking, resulting in a yellowish coloration, while WJ-TA-ox membranes became brown, indicating the occurrence of the cross-linking processes (Fig. 1A). The degree of cross-linking of the WJ-TA and WJ-TA-ox membranes was determined using the ninhydrin assay. WJ-TA-ox membranes had at least 2-fold higher cross-linking degree than WJ-TA ($p < 0.0001$, Table 1).

The WJ-TA and WJ-TA-ox membranes were further characterized by Fourier Transformed Infrared (FTIR) spectroscopy (Fig. 1B). Decellularized WJ membranes showed amides I, II and III bands at 1628 cm^{-1}, 1540 cm^{-1} and 1230 cm^{-1}, respectively, indicating that the basic structure of the collagen fiber is maintained. On WJ-TA membranes, the presence of TA was confirmed by the following peaks: 1720 (C=O ester), 1327 (phenolic C—OH) and 1195 cm^{-1} (phenolic C—OH) [30,31]. A slight shift towards lower values was observed in the amide I and III absorption peaks, indicating that the hydrogen bonding occurs between TA molecules and amine groups of collagen [24], with a preservation of the secondary structure of the collagen [32]. After $NaIO_4$ treatment, the peak of TA at 1195 cm^{-1} decreased due to the oxidation of phenolic hydroxyl groups into quinone moieties [33]. In the amide I band, a shoulder appeared at 1643 cm^{-1} (C=N stretching mode of imines), supporting the occurrence of a Schiff-base reaction between quinone moieties of TA and amine groups of collagen [34]. The Michael addition type reaction is also supported by the shoulder at 1520 cm^{-1} in the amide II band region, attributed to NH bending [34] due to the conversion of some primary amines into secondary ones. Taken together, these results suggest that TA-ox could simultaneously cross-link multiple collagen fibers, increasing the compactness of the collagen fibers and thus increasing the density of the collagen network [35]. The ECM structure, investigated by hematoxylin-eosin-saffron (HES) stained sections indicated that WJ membranes appear pink, while WJ-TA became more purple-red (Fig. 1C). WJ-TA-ox membranes showed a pronounced and consistent purple-red color confined to the membrane borders,

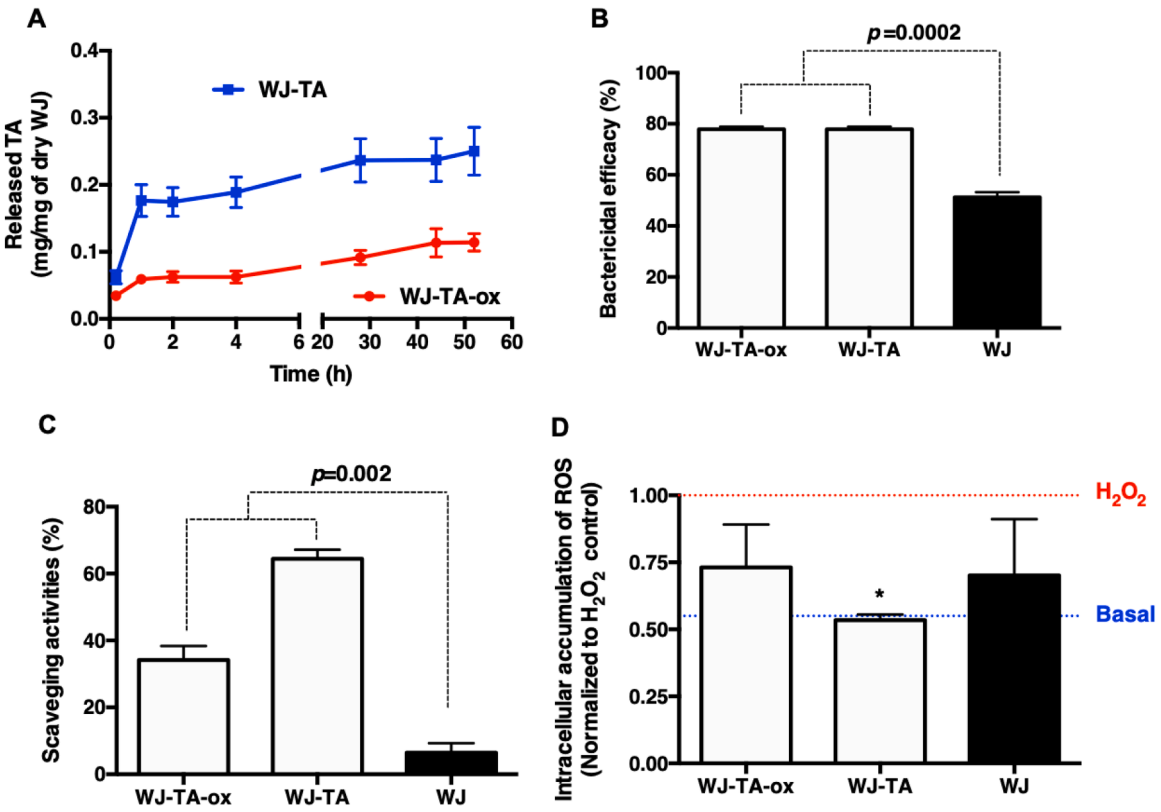

Fig. 2. Biological activities of the released tannic acid from cross-linked Wharton's jelly membranes. A: TA Kinetic release from WJ-TA-ox (red line) and WJ-TA (blue line). B: Bactericidal efficacy of WJ-TA-ox, WJ-TA and WJ on S. aureus strain. C: *In vitro* antioxidant activity of the WJ-TA-ox, WJ-TA and WJ extracts. D: Normalized mean intensity of fluorescence of the intracellular fibroblast accumulated ROS after 24 h of culture in the presence of WJ-TA-ox, WJ-TA and WJ and exposure for 3 h to H_2O_2. Dashed red and blue lines indicate respectively the positive and negative controls. *$p = 0.01$ vs. positive control (Mann & Whitney test).

suggesting a limited diffusion of $NaIO_4$ into the WJ membrane. After cross-linking, scanning electron microscopy (SEM) images showed that the collagen appeared to be more densely packed with the presence of a pearl necklace-*like* structures, a signature of the formation of hydrophobic pockets (Fig. 1D). Indeed, the hydrophobic amino acid side chains on collagen such as aromatic ring, pyrrolidine ring, and aliphatic chain are prone to form a hydrophobic pocket. In the presence of TA, the aromatic rings of galloyl units on TA attract the hydrophobic groups on collagen, forming hydrophobic interactions and hydrophobic pockets [36]. The size of the globular structures of TA/collagen complexes [37] appeared to be larger and more abundant in WJ-TA compared to WJ-TA-ox membrane.

Swelling capacity and the moisture content are important considerations in the biomedical field. Appropriate swelling is required to absorb blood and exudate from the wounds. A high water content (> 80%) is expected to provide a good environment for cells, with additional properties such as antimicrobial properties [38]. It is well known that a higher degree of cross-linking results in low swelling properties. Indeed, the cross-linking of WJ by TA and TA-ox resulted in a notable reduction in the swelling capabilities and in water content ($p < 0.002$, Table 1), with a slight decrease between WJ-TA-ox and WJ-TA ($p = 0.17$). Taken together, these results suggest that the TA treatment may have an effect on the pore size/interconnectivity of the collagen fibers [39]. The increase in the degree of cross-linking resulted in a denser collagen network with smaller pores between collagen fibers [40]. Consequently, water molecules had difficulty entering the inner part of the collagenous network. To evaluate the membrane porosity, samples were submerged in absolute ethanol, preventing the collagen hydration [8]. The results showed that the total porosity of the WJ-TA-ox membranes was close to WJ-TA ones ($p > 0.99$), but significantly lower than that of WJ membranes ($p < 0.002$, Table 1). Despite the decrease in the total porosity, the structure of the cross-linked WJ membranes remained highly interconnected (> 80%) and suitable for cell colonization [41]. The decrease in the swelling ratio of both WJ-TA-ox and WJ-TA could also be attributed to the decrease in hydrophilicity of the membranes. Indeed, by measuring the water angle contact, the surface of the WJ-TA membranes became hydrophobic as the angle contact reached 57 ± 5° ($p < 0.0003$), whereas the angle contact of the WJ-TA-ox was close to that of WJ ($p = 0.07$, Table 1).

Recently, it has been reported that TA molecules can strongly or loosely interact with gelatin (denatured collagen), leading to its release under physiological conditions [42]. Therefore, the amount of diffused TA from WJ-TA-ox and WJ-TA membranes was assessed for 52 h (Fig. 2A). The results showed a rapid release of TA from the WJ-TA after 1 h of incubation in PBS ($p < 0.004$). Over the next 52 h, TA content continued to increase at a slower rate, reaching 0.25 ± 0.08 mg/mg of dry sample ($p < 0.002$). The rate of TA release from WJ-TA-ox membrane was slower than that of WJ-TA membrane, reaching 0.11 ± 0.03 mg/mg of dry sample ($p < 0.002$). It is expected that the released TA would exert its antibacterial properties and antioxidant ability [38]. The antibacterial activities of WJ-TA-ox and WJ-TA membranes were firstly evaluated against *Staphylococcus aureus* (*S. aureus*). As published previously, decellularized WJ membranes [7] and TA [37] possess antibacterial effects against *Staphylococcus* Gram positive bacteria. The bactericidal activity was determined by incubating *S. aureus* in the presence of samples for 24 h, and then measuring the number of live bacteria. Compared to the initially inoculated bacteria, the WJ-TA-ox and WJ-TA membranes significantly reduced the number of live bacteria, reaching 10 CFU/mL, after 24 h of contact ($p < 0.0001$, Fig. SI-1A). Killing efficiency was calculated by comparing the number of CFU formed in the presence and the absence of samples (Fig. 2B). The results showed a high bactericidal activity of WJ-TA-ox and WJ-TA compared

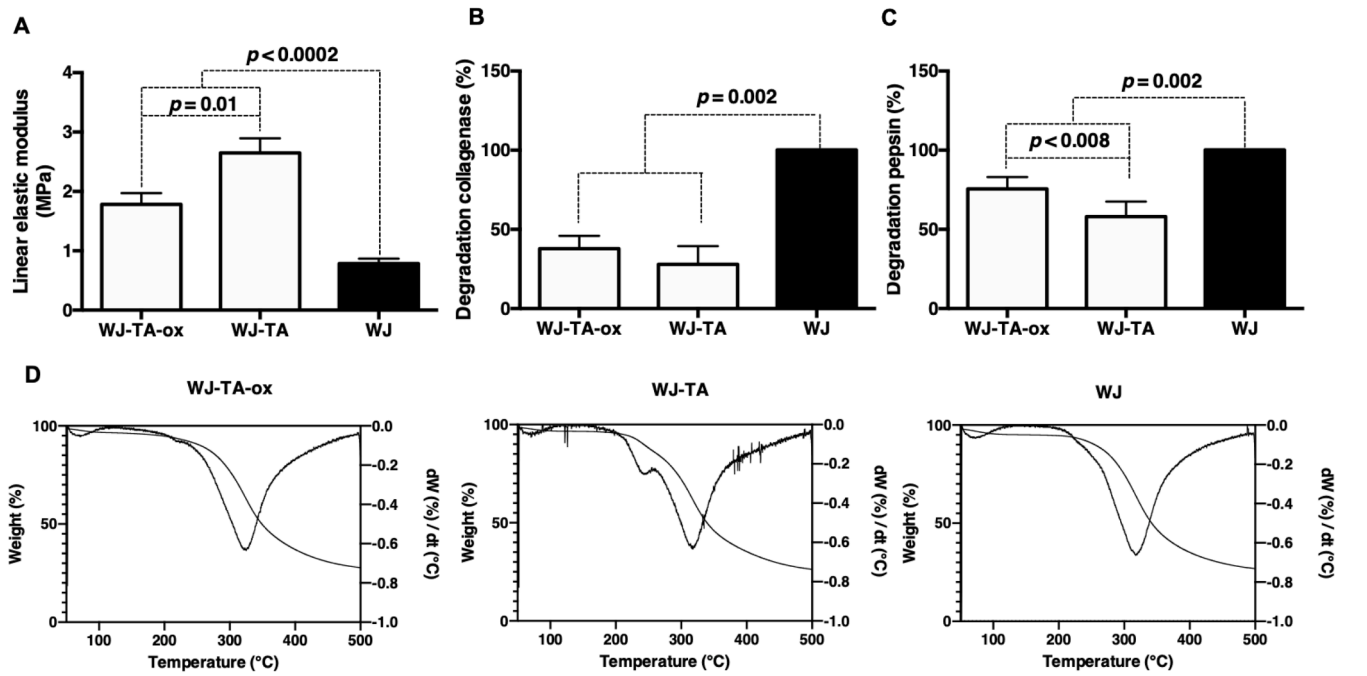

Fig. 3. Mechanical characteristic and biological stability of the tannic acid cross-linked Wharton's jelly. A: Linear elastic modulus of WJ-TA-ox and WJ-TA hydrated membranes undergoing small strain, showing no noticeable difference in the cross-linked WJ mechanical response *versus* WJ. B and C: Collagenase and pepsin degradation assay, showing an increase in the resistance of WJ to the enzymatical actions after TA cross-link. D: Thermogravimetric analyses of WJ-TA-ox and WJ-TA membranes, indicating a thermal resistance of the collagen degradation after TA cross-link. .

to WJ membranes (~ 80% *versus* 50%, $p = 0.002$). The antibacterial effectiveness of TA could be explained by its ability to pass through the bacterial wall, causing the bacterial destruction by interfering with the metabolism of the *Staphylococcus*'s metabolism (*i.e.* iron ion chelation or complexes with oxidoreductase enzyme) [43,44].

The antioxidant activity of the released TA was secondly evaluated, using 2,2-diphenyl-1-picrylhydrazyl (DPPH) radical scavenging assay. A dose-dependent increase in the radical scavenging activity was observed for both WJ-TA-ox and WJ-TA, with a higher release from the WJ-TA membranes (Fig. SI-1B). However, the radical scavenging effect on DPPH and the reactive oxygen species (ROS) removal efficiency were higher for the WJ-TA-ox and WJ-TA extracts compared to WJ extracts ($p < 0.0001$, Fig. 2C). Taken together, these results indicate that the released TA from WJ-TA has free radical scavenging activity. ROS, two electron reduction products of oxygen, including hydrogen peroxide, are maintained in a dynamic balance in living cells. Excessive oxidative stress resulting from the accumulation of intracellular ROS deregulates the antioxidant defense system, leading to cell death by damaging cellular components [45]. Fibroblasts stimulated by H_2O_2 were validated as oxidative stress injured cell model to study the antioxidative activity *in vitro* [46]. Scavenging the abnormal accumulation of intracellular ROS in fibroblasts after H_2O_2 stimulation was evaluated in the presence of freeze dried membranes. The intracellular accumulation of ROS in the presence of WJ-TA membrane was weaker than H_2O_2-stimulated cell control ($p < 0.006$, Fig 2D). WJ-TA membrane showed a better ability to scavenge excessive ROS accumulation compared to WJ-TA-ox membrane, probably due to the higher amount of TA released into the extracellular medium (0.28 ± 0.05 and 0.78 ± 0.22 mM for WJ-TA-ox and WJ-TA membranes respectively, $p < 0.002$).

As mentioned above, the TA cross-linking is expected to increase the mechanical performance of the WJ membrane and avoid its rapid enzymatical degradation. The linear elastic modulus, a linear approximation of the stress-strain curve that represents the linear elastic response of the membrane, was monitored in the wet state at an average strain load of 1.6%, avoiding the sample damage (toe region of Fig. SI-2). The results showed a significant increase in the linear elastic modulus of the WJ-TA-ox and WJ-TA when compared to the WJ membranes (at least 2-fold increase, $p < 0.007$, Fig. 3A). Surprisingly, despite the increase in the cross-linking degree of WJ-TA-ox, the linear elastic modulus was significantly lower than that of WJ-TA membranes (at least 0.7-fold decrease, $p = 0.04$). These results suggest that the mechanical stress breaks the sacrificial bonds (*i.e.* hydrogen bonds) of WJ-TA, leaving the collagen chains intact and allowing the collagen network to resist fracture and stretch [47].

The relative degree of enzymolysis degree of the samples was also investigated after 48 h of incubation in collagenase or pepsin. According to our results, WJ-TA-ox and WJ-TA membranes were highly resistant to the degradation by the collagenase, as indicated by the significantly lower degradation rates compared to WJ membranes (mass loss of $28 \pm 10\%$, $38 \pm 7\%$ and 100 % respectively, $p < 0.002$, Fig. 3B). Interestingly, the WJ-TA-ox and WJ-TA membranes appeared to be less resistant to the action of pepsin in comparison with collagenase (mass loss of $58 \pm 8\%$ and $75 \pm 6\%$ after 48 h of incubation, respectively, Fig. 3C). In addition, significantly higher degradation rates of WJ-TA membrane compared to WJ-TA-ox membrane was observed (at least 1.3-fold increase, $p < 0.008$). Collagenase cleaves the peptide bonds between repeated glycine-proline-X (X being often proline or hydroxyproline) [48]. TA cross-link may reduce access of collagenase to potential cleavage sites after its interaction with the glycine amino group [49]. The increase in the collagenase resistance of TA cross-linked membranes could also be due to the released TA, which may bind the protein collagenase, rendering it less active. In contrast, TA cross-linking did not prevent the potential cleavage sites (*i.e.* telopeptide regions of tropocollagen) from pepsin attack. These results suggested that the cross-linking did not affect the amino acid sequence of the telopeptide region, that remains accessible to the pepsin action. To confirm the minimal effect of TA treatment, the freeze-dried samples were also characterized by thermogravimetric analysis (TGA). The loss of absorbed water, observed between 50 °C and 200 °C, was 4 and 5% for WJ-TA-ox and WJ-TA, respectively *vs.* 6% for WJ membranes. In the next stage of thermal decomposition (200 °C to 400 °C), mass losses of 57% (WJ-TA-ox) and 60% (WJ-TA) *versus* 62% (WJ) were observed (Fig. 3D). The calculated

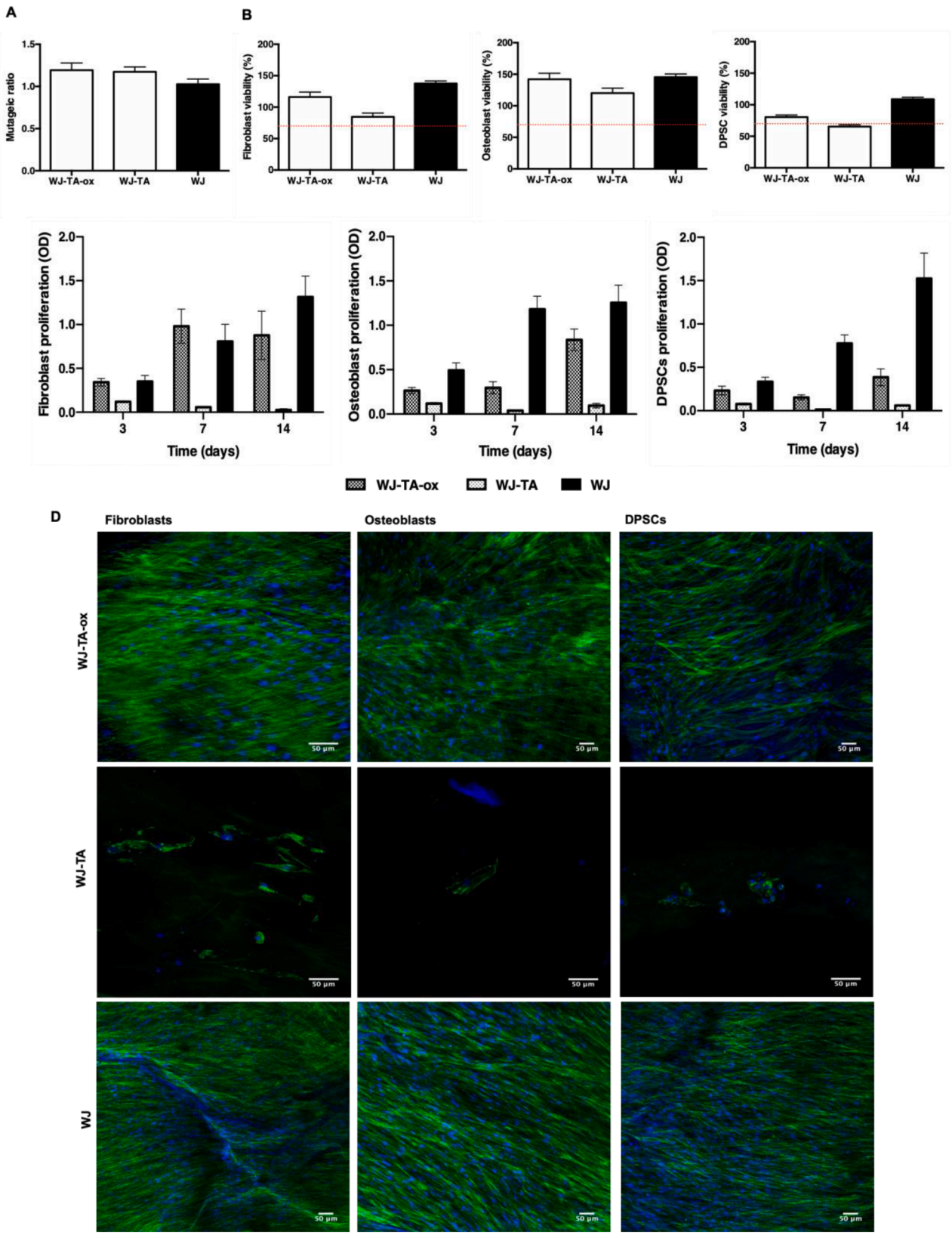

Fig. 4. *In vitro* biocompatibility of the tannic acid cross-linked Wharton's jelly membranes. A: Ames assay and B: Viability assay on fibroblasts, osteoblasts and dental pulp stromal cells (DPSCs). Dashed red line, indicating the cytotoxicity threshold, confirms the biocompatibility of TA cross-linked WJ membranes. C: Fibroblasts, osteoblasts and DPSCs proliferation assay on WJ-TA-ox and WJ-TA membranes, indicating the absence of cell proliferation on WJ-TA one. D: Laser scanning confocal microscopy views of fibroblasts, osteoblasts and DPSCs cultured on WJ-TA-ox and WJ-TA membranes labelled with phalloidin (in green) and DAPI (in blue). Scale bars = 50 µm. .

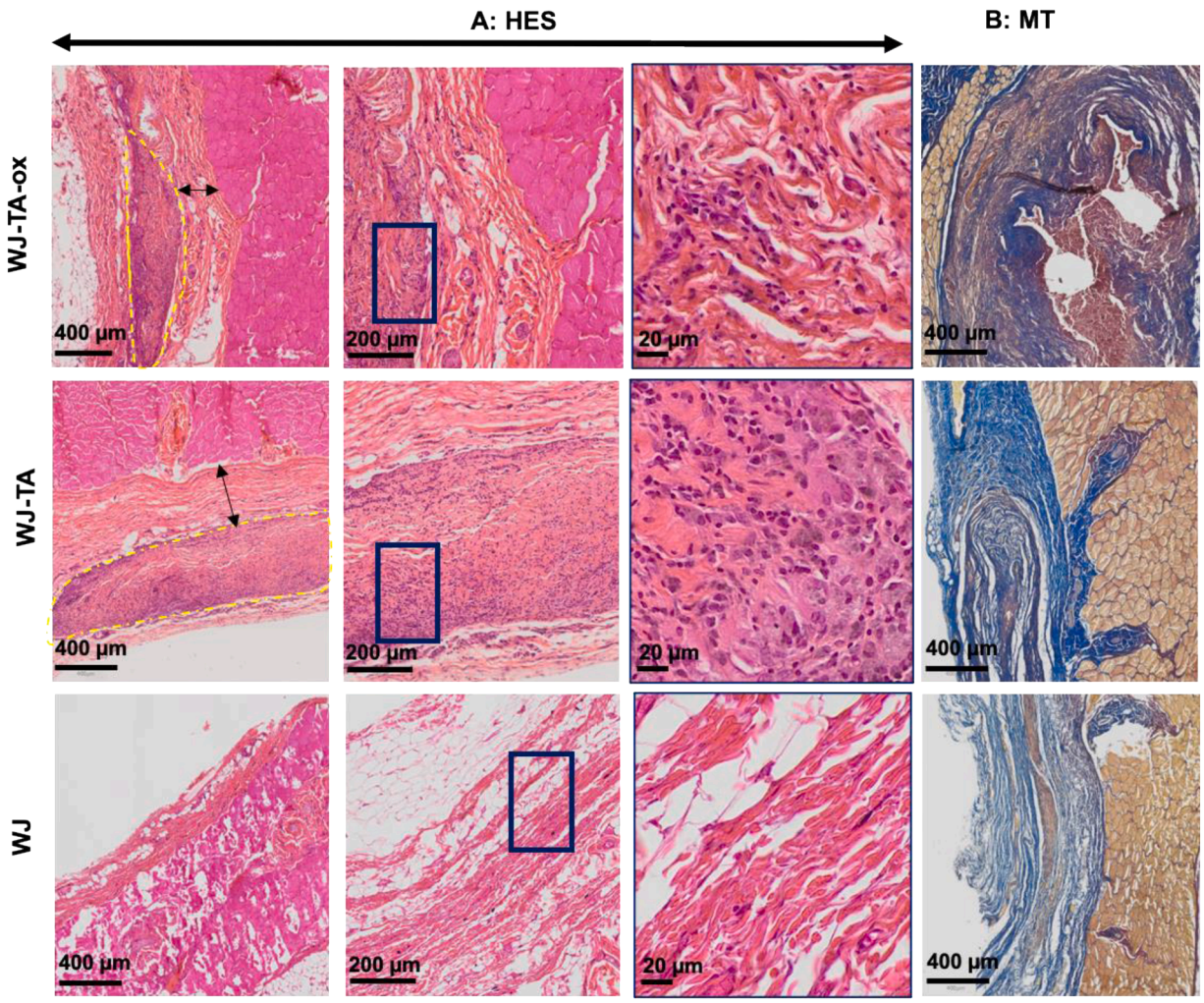

Fig. 5. *In vivo* biocompatibility of the tannic acid cross-linked Wharton's jelly. A and B: HES and MT staining of the explanted samples after seven weeks of implantation. First, second and third lines represent WJ-TA-ox, WJ-TA and WJ explanted membranes, respectively. Dashed delimitations indicate the implanted WJ-TA-ox and WJ-TA membranes. Pictures delimited by blue lines represents a higher magnification of the blue square. Black double arrows indicate fibrotic capsule Scale bars = 400, and 200 and 20 µm.

temperatures at 50% weight losses ($T°_{50}$) increased from 341 °C to 349 °C and the residuals (%) at 500 °C ($R\%_{500}$) was 26.71% and 27.65%, for WJ and WJ-TA-ox, respectively. These results suggest that the thermal resistance of collagen degradation for WJ-TA-ox membrane could be explained by the strong interaction between oxidized phenolic compounds and functional groups on collagen fibers [50].

The above cited results demonstrated that TA could be released from the WJ. In the following, the potential risks of adverse effects of the TA release was investigated by using *His⁻ S. typhimurium strains* according to the genotoxicity ISO/EN 10,993 part 3 and OECD 471 guidelines and primary cultured cells (*i.e.* dental pulp stem cells, fibroblasts and osteoblasts), according to cytotoxicity ISO/EN 10,993 part 5 guidelines. The calculated mutagenic ratio remained above the threshold of 2 (*vs.* water blank control, Fig. 4A), demonstrating the absence of a potential mutagenic effect of the released TA on *His⁻ S. typhimurium* [51]. The viability of fibroblasts, osteoblasts and dental pulp derived stromal cells (DPSCs) in the presence of WJ-TA-ox and WJ-TA membranes remained above the threshold of 70% of cell viability (*vs.* plastic culture positive control, Fig. 4B), threshold considered as an indicator of cytotoxic phenomenon. Taken together, these results demonstrated the absence of both genotoxic and cytotoxic effect of TA and $NaIO_4$.

The preparation of an appropriate scaffold that mimics the native microenvironment of cells is one of the key elements in regenerative medicine. It is generally admitted that the increase in the surface wettability leads to a decrease in the cell adhesion [52]. For a potential use of WJ-TA-ox and WJ-TA membranes as a bone tissue scaffold, the proliferation of fibroblasts, osteoblasts and DPSCs was monitored. The proliferation of cells within WJ-TA-ox membranes increased significantly in a time-dependent manner starting from day 7, 10, and 14 (Fig. 4C). Fibroblasts reached a plateau at day 10, whereas osteoblasts and DPSCs showed an exponential growth. Compared to WJ membranes, all the studied cells had a lower growth on the WJ-TA-ox, while they failed to proliferate on the WJ-TA membranes. These results are in contradiction with Zhu et al. [47] who demonstrated beneficial effects of TA on the proliferation of HOK cell line, but are in agreement with He et al. who attributed the low bone marrow derived stromal cells proliferation to the non-specific negative interactions between TA and cell membrane proteins [53]. The morphological examination of adhered cells on WJ-TA-ox showed an elongated cell morphology as observed for the WJ membrane (Fig. 4D). However, the penetration of cells within the WJ-TA-ox membrane seemed limited (Fig. SI-3).

To investigate the host's response, the membranes were implanted subcutaneously, according to ISO/EN 10,993 part 6 guideline. Based on the 3Rs principles as well as practical issues, each sample was implanted in the same animal. Wounds were closed in all animals without infection or other complications. Hair growth in the surgical area was normal. Seven weeks after implantation, WJ-TA-ox and WJ-TA membranes were not degraded, whereas a complete resorption of WJ membrane was

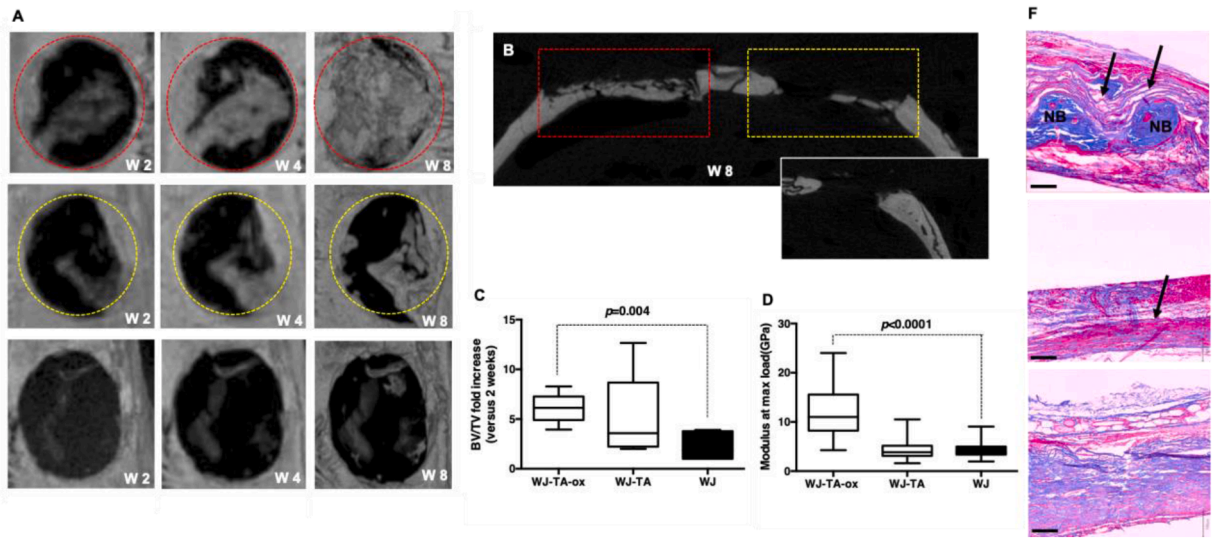

Fig. 6. Parietal bone regeneration in the presence of tannic acid cross-linked Wharton's jelly. A: μ-CT coronal views of de novo parietal bone in the presence of WJ-TA-ox (upper line, dashed red rings), WJ-TA (middle line, dashed yellow rings) and WJ membranes (lower line) after 2 and 4 weeks (35 μm in resolution) and 8 weeks (17.9 μm in resolution). B: μ-CT trans-axial views of the de novo parietal bone in the presence of WJ-TA-ox (dashed red rectangle), WJ-TA (dashed yellow rectangle) and WJ membranes (insert) after 8 weeks (17.9 μm in resolution). C: Quantitative μ–CT results, indicating bone volume/total volume ratio (BV/TV) and normalized to 2 weeks results ($n = 6$, Mann–Whitney test). D: Modulus at max load, measured by nanoindentation ($n = 4$, Mann–Whitney test). F: Resin-embedded sections of the explanted parietal bone in the in the presence of WJ-TA-ox (upper line), WJ-TA (middle line) and raw WJ (lower line). Black arrows indicate the presence of implanted WJ. NB = newly formed bone (scale bars = 100 μm).

observed (Fig. 5A). Both WJ-TA-ox and WJ-TA membranes were colonized by a reparative granulation tissue (macrophages and fibroblasts). WJ-TA-ox membrane induced a neglecting capsule fibrosis compared to WJ-TA one (Fig. 5B). Furthermore, liver, kidney and bladder were collected for HES staining; no lesions or inflammatory infiltration were observed in these tissues (Fig. SI-4). Despite the chemical cross-linking, WJ retained its "unrecognized as a foreign material" status [54] as no calcification or other adverse recipient reaction was observed.

Osseointegration is a complex process that requires the collaboration of multiple cells from diverse systems (immune, bone and vascular cells) [55]. To investigate the ability of the TA cross-linked WJ membrane to induce bone regeneration, a rat parietal (*i.e.*, calvaria) bone defect model was used. Rats received in the right side WJ-TA-ox and at the left side the WJ-TA. This paper share the same control that the previous papers [7,28]. The rats were continuously monitored after the surgery until recovery. Gross observation of the animals after surgery showed no complications. All groups exhibited a good tissue compatibility and no adverse events such as a foreign body reaction nor infection were observed throughout the eight-weeks study period. Microtomography (μ–CT) analysis was carried out for the structural and quantitative assessments of the *de novo* bone.

μ–CT coronal views showing the temporal evolution of the bone healing indicated almost complete closure of the defect in the presence of WJ-TA-ox membranes compared to WJ-TA ones (Fig. 6A). The μ–CT trans-axial views at higher resolution showed an increase in bone volume after eight weeks of implantation in the presence of WJ-TA-ox membranes (Fig. 6B). To confirm these observations, quantitative analysis of bone volume/total volume ratio was performed. WJ-TA-ox significantly out-performed the WJ-TA and WJ membranes in terms of the *de novo* bone formation with 2.6-fold increase in bone volume compared to WJ membrane ($p < 0.004$, Fig. 6C). The increase in bone volume could reflect a stiffer bone. Therefore, the mechanical performance of the *de novo* bone was evaluated at a nanoscale. Nanoindentation in the center of the sample showed that the modulus was significantly higher in bone formed in the presence of WJ-TA-ox membrane (2.7 fold increase, $p < 0.0001$, Fig. 6D). Finally, MT staining was used to further evaluate *de novo* bone on resin embedded-calcified parietal bones (Fig. 6F). The presence of *de novo* bone nodules at the defect site confirmed the superiority of the WJ-TA-ox compared to WJ-TA and WJ membranes where the bone defect was filled with a loose connective tissue. In addition, substantial fragments of the WJ-TA-ox and WJ-TA were still visible in the bone defect after eight weeks of implantation. To sum up, these *in vivo* data revealed that WJ-TA-ox membranes boost the bone regeneration. The subcutaneous implantation of tannic acid cross-linked WJ membranes did not show an ectopic calcification after 56 days of implantation. Taken together these results suggest the absence of a direct stimulation of osteogenesis (*i.e.* osteoinduction and osteoconduction) of the release tannic acid. Thus, the osteogenic capability of the TA cross-linked WJ membranes could be attributed to the osteo-immunomodulatory action of the released tannic acid, through the attenuation of the excessive accumulation of ROS and also by inducing the macrophage polarization toward osteo-immunoregulatory profile [56].

In conclusion, the resulting WJ-TA-ox membrane showed an increase in the enzymatic and thermal degradation resistance, and an increase in the mechanical elasticity. WJ-TA-ox membrane had the ability to kill bacteria and scavenge reactive oxygen species, thereby maintaining cell viability, and promoting cell proliferation. WJ-TA-ox multifunctional membrane thus provides a supportive microenvironment, with a unique combination of properties, for the endogenous regeneration of parietal bone defects and may serve as a promising biomaterial for future clinical treatment aimed at improving the bone healing.

CRediT authorship contribution statement

L. Scomazzon: Formal analysis, Data curation. **F. Lemaire:** Formal analysis, Data curation. **M. Dubus:** Formal analysis, Data curation, Conceptualization. **J. Braux:** Validation, Methodology, Conceptualization. **C. Terryn:** Visualization, Formal analysis. **A. Baldit:** Formal analysis, Data curation, Conceptualization. **J.S. Lecomte:** Visualization, Validation. **Q. Carboué:** Formal analysis, Data curation. **C. Guillaume:** Formal analysis. **N. Bouland:** Formal analysis. **E. Brenet:** Writing – review & editing, Visualization, Validation. **F. Boulmedais:** Writing – review & editing, Writing – original draft, Funding acquisition, Conceptualization. **C. Mauprivez:** Visualization, Validation, Supervision, Conceptualization. **H. Kerdjoudj:** Writing – review & editing,

Writing – original draft, Supervision, Project administration, Funding acquisition, Conceptualization.

Declaration of competing interest

The authors declare that they have no conflict of interest.

Data availability

Data will be made available on request.

Acknowledgments

This research was funded by Région Grand Est (ERMES project). The authors are very grateful to the staff of the Core PICT, and URCANim (Pr. S. Dukic and Dr. S. Audonnet) from URCA and MécaRhéo from LEM3 (Université de Lorraine). The authors would also like to thank especially Dr. Marius Colin for the microbiological assays and Jennalyn Philipps from New York university for the English revision.

Supplementary materials

Supplementary material associated with this article can be found, in the online version, at doi:10.1016/j.apmt.2024.102241.

References

[1] A. Neishabouri, A. Soltani Khaboushan, F. Daghigh, A.M. Kajbafzadeh, M. Majidi Zolbin, Decellularization in tissue engineering and regenerative medicine: evaluation, modification, and application methods, Front. Bioeng. Biotechnol. 10 (2022) 805299, https://doi.org/10.3389/fbioe.2022.805299.

[2] E. Garreta, R. Oria, C. Tarantino, M. Pla-Roca, P. Prado, F. Fernández-Avilés, J. M. Campistol, J. Samitier, N. Montserrat, Tissue engineering by decellularization and 3D bioprinting, Mater. Today. 20 (2017) 166–178, https://doi.org/10.1016/j.mattod.2016.12.005.

[3] U. Mendibil, R. Ruiz-Hernandez, S. Retegi-Carrion, N. Garcia-Urquia, B. Olalde-Graells, A. Abarrategi, Tissue-specific decellularization methods: rationale and strategies to achieve regenerative compounds, Int. J. Mol. Sci. 21 (2020) 5447, https://doi.org/10.3390/ijms21155447.

[4] N. Beheshtizadeh, M. Gharibshahian, Z. Pazhouhnia, M. Rostami, A.R. Zangi, R. Maleki, H.K. Azar, V. Zalouli, H. Rajavand, A. Farzin, N. Lotfibakhshaiesh, F. Sefat, M. Azami, T.J. Webster, N. Rezaei, Commercialization and regulation of regenerative medicine products: promises, advances and challenges, Biomed. Pharmacother. 153 (2022) 113431, https://doi.org/10.1016/j.biopha.2022.113431.

[5] F. Gindraux, N. Hofmann, M. Agudo-Barriuso, M. Antica, P.S. Couto, M. Dubus, S. Forostyak, L. Girandon, R. Gramignoli, M. Jurga, S. Liarte, R. Navakauskiene, V. Shablii, X. Lafarge, F.J. Nicolás, Perinatal derivatives application: identifying possibilities for clinical use, Front. Bioeng. Biotechnol. 10 (2022) 1–20, https://doi.org/10.3389/fbioe.2022.977590.

[6] M.C. Moore, A. Van De Walle, J. Chang, C. Juran, P.S. McFetridge, Human perinatal-derived biomaterials, Adv. Healthc. Mater. 6 (2017), https://doi.org/10.1002/adhm.201700345.

[7] M. Dubus, L. Scomazzon, J. Chevrier, C. Ledouble, A. Baldit, J. Braux, F. Gindraux, C. Boulagnon, S. Audonnet, M. Colin, H. Rammal, C. Mauprivez, H. Kerdjoudj, Antibacterial and immunomodulatory properties of acellular Wharton's jelly matrix, Biomedicines 10 (2022) 227, https://doi.org/10.3390/biomedicines10020227.

[8] M. Dubus, L. Scomazzon, J. Chevrier, A. Montanede, A. Baldit, C. Terryn, F. Quilès, C. Thomachot-Schneider, S.C. Gangloff, N. Bouland, F. Gindraux, H. Rammal, C. Mauprivez, H. Kerdjoudj, Decellularization of Wharton's jelly increases its bioactivity and antibacterial properties, Front. Bioeng. Biotechnol. 10 (2022) 828424, https://doi.org/10.3389/fbioe.2022.828424.

[9] C. Wang, G. Li, K. Cui, Z. Chai, Z. Huang, Y. Liu, S. Chen, H. Huang, K. Zhang, Z. Han, Y. Li, G. Yu, Z.C. Han, N. Liu, Z. Li, Sulfated glycosaminoglycans in decellularized placenta matrix as critical regulators for cutaneous wound healing, Acta Biomater 122 (2021) 199–210, https://doi.org/10.1016/j.actbio.2020.12.055.

[10] Z. Kočí, K. Výborný, J. Dubišová, I. Vacková, A. Jäger, O. Lunov, K. Jiráková, S. Kubinová, Extracellular matrix hydrogel derived from human umbilical cord as a scaffold for neural tissue repair and its comparison with extracellular matrix from porcine tissues, Tissue Eng. Part C Methods 23 (2017) 333–345, https://doi.org/10.1089/ten.tec.2017.0089.

[11] A. Basiri, M. Farokhi, M. Azami, S. Ebrahimi-Barough, A. Mohamadnia, M. Rashtbar, E. Hasanzadeh, N. Mahmoodi, M. Baghaban Eslaminejad, J.A. Ai, Silk fibroin/decellularized extract of Wharton's jelly hydrogel intended for cartilage tissue engineering, Prog. Biomater. 8 (2019) 31–42, https://doi.org/10.1007/s40204-019-0108-7.

[12] L. Penolazzi, M. Pozzobon, L.S. Bergamin, S. D'Agostino, R. Francescato, G. Bonaccorsi, P. De Bonis, M. Cavallo, E. Lambertini, R. Piva, Extracellular matrix from decellularized Wharton's jelly improves the behavior of cells from degenerated intervertebral disc, Front. Bioeng. Biotechnol. 8 (2020) 262, https://doi.org/10.3389/fbioe.2020.00262.

[13] M. Dubus, H. Kerdjoudj, L. Scomazzon, J. Sergheraert, C. Mauprivez, R. Rahouadj, A. Baldit, Mechanical behaviour of a membrane made of human umbilical cord for dental bone regenerative medicine, Comput. Methods Biomech. Biomed. Engin. 23 (2020) S88–S90, https://doi.org/10.1080/10255842.2020.1812169.

[14] S. Odet, C. Meyer, C. Gaudet, E. Weber, J. Quenot, S. Derruau, S. Laurence, L. Bompy, M. Girodon, B. Chatelain, C. Mauprivez, E. Brenet, H. Kerdjoudj, N. Zwetyenga, P. Marchetti, A.S. Hatzfeld, D. Toubeau, F. Pouthier, X. Lafarge, H. Redl, M. Fenelon, J.C. Fricain, R. Di Pietro, C. Ledouble, T. Gualdi, A. L. Parmentier, A. Louvrier, F. Gindraux, Tips and tricks and clinical outcome of cryopreserved human amniotic membrane application for the management of medication-related osteonecrosis of the Jaw (MRONJ): a pilot study, Front. Bioeng. Biotechnol 10 (2022) 936074, https://doi.org/10.3389/fbioe.2022.936074.

[15] F. Safari, N. Fani, D. Eglin, M. Alini, M.J. Stoddart, M. Baghaban Eslaminejad, Human umbilical cord-derived scaffolds for cartilage tissue engineering, J. Biomed. Mater. Res. A 107 (2019) 1793–1802, https://doi.org/10.1002/jbm.a.36698.

[16] Y. Xu, L. Duan, Y. Li, Y. She, J. Zhu, G. Zhou, G. Jiang, Y. Yang, Nanofibrillar decellularized Wharton's jelly matrix for segmental tracheal repair, Adv. Funct. Mater 30 (2020) 1910067, https://doi.org/10.1002/adfm.201910067.

[17] J. Adamowicz, M. Pokrywczyńska, J. Tworkiewicz, T. Kowalczyk, S. van Breda, D. Tyloch, T. Kloskowski, M. Bodnar, J. Skopinska-Wisniewska, A. Marszałek, M. Frontczak-Baniewicz, T.A. Kowalewski, T. Drewa, New amniotic membrane based biocomposite for future application in reconstructive urology, PLoS ONE 11 (2016) e0146012, https://doi.org/10.1371/journal.pone.0146012.

[18] M. Pozzobon, S. D'Agostino, M.G. Roubelakis, A. Cargnoni, R. Gramignoli, S. Wolbank, F. Gindraux, S. Bollini, H. Kerdjoudj, M. Fenelon, R. Di Pietro, M. Basile, V. Borutinskaitė, R. Piva, A. Schoeberlein, G. Eissner, B. Giebel, P. Ponsaerts, General consensus on multimodal functions and validation analysis of perinatal derivatives for regenerative medicine applications, Front. Bioeng. Biotechnol. 10 (2022) 961987, https://doi.org/10.3389/fbioe.2022.961987.

[19] A. Aratikatla, N. Maffulli, H.C. Rodriguez, M. Gupta, A.G. Potty, S.F. El-Amin, A. Gupta, Allogenic perinatal tissue for musculoskeletal regenerative medicine applications: a systematic review protocol, J. Orthop. Surg. 17 (2022) 307, https://doi.org/10.1186/s13018-022-03197-z.

[20] N. Venkatesan, V. Lavu, S.K. Balaji, Clinical efficacy of amniotic membrane with biphasic calcium phosphate in guided tissue regeneration of intrabony defects- a randomized controlled clinical trial, Biomater. Res. 25 (2021) 15, https://doi.org/10.1186/s40824-021-00217-7.

[21] A. Bigham, V. Rahimkhoei, P. Abasian, M. Delfi, J. Naderi, M. Ghomi, F. Dabbagh Moghaddam, T. Waqar, Y. Nuri Ertas, S. Sharifi, N. Rabiee, S. Ersoy, A. Maleki, E. Nazarzadeh Zare, E. Sharifi, E. Jabbari, P. Makvandi, A. Akbari, Advances in tannic acid-incorporated biomaterials: infection treatment, regenerative medicine, cancer therapy, and biosensing, Chem. Eng. J. 432 (2022) 134146, https://doi.org/10.1016/j.cej.2021.134146.

[22] H. Jafari, P. Ghaffari-Bohlouli, S.V. Niknezhad, A. Abedi, Z. Izadifar, R. Mohammadinejad, R.S. Varma, A. Shavandi, Tannic Acid: a versatile polyphenol for design of biomedical hydrogels, J. Mater. Chem. B 10 (2022) 5873–5912, https://doi.org/10.1039/D2TB01056A.

[23] E. Haslam, T.H. Lilley, Y. Cai, R. Martin, D. Mangnolato, Traditional herbal medicines - the role of polyphenols, Planta Med 55 (1989) 1–8, https://doi.org/10.1055/s-2006-961764.

[24] L. Wu, H. Shao, Z. Fang, Y. Zhao, C.Y. Cao, Q. Li, Mechanism and effects of polyphenol derivatives for modifying collagen, ACS Biomater. Sci. Eng. 5 (2019) 4272–4284, https://doi.org/10.1021/acsbiomaterials.9b00593.

[25] S. Ge, N. Ji, S. Cui, W. Xie, M. Li, Y. Li, L. Xiong, Q. Sun, Coordination of covalent cross-linked gelatin hydrogels via oxidized tannic acid and ferric ions with strong mechanical properties, J. Agric. Food Chem. 67 (2019) 11489–11497, https://doi.org/10.1021/acs.jafc.9b03947.

[26] A. Baldit, M. Dubus, J. Sergheraert, H. Kerdjoudj, C. Mauprivez, R. Rahouadj, Biomechanical tensile behavior of human Wharton's jelly, J. Mech. Behav. Biomed. Mater. 126 (2022) 104981, https://doi.org/10.1016/j.jmbbm.2021.104981.

[27] V. Gribova, J.M.A. Dominguez, A. Morin, J.S. Diaz, P. Lavalle, N.E. Vrana, Miniaturized genotoxicity evaluation system for fast biomaterial-related risk assessment, Anal. Methods 15 (2023) 1584–1593, https://doi.org/10.1039/D2AY01873J.

[28] M. Dubus, L. Scomazzon, C. Ledouble, J. Braux, A. Beljebbar, L. Van Gulick, A. Baldit, C. Gorin, H. Alem, N. Bouland, M. Britton, J. Schiavi, T.J. Vaughan, C. Mauprivez, H. Kerdjoudj, Hybrid Mineral/Organic material induces bone bridging and bone volume augmentation in rat calvarial critical size defects, Cells 11 (2022) 2865, https://doi.org/10.3390/cells11182865.

[29] H. Liang, B. Zhou, D. Wu, J. Li, B. Li, Supramolecular design and applications of polyphenol-based architecture: a review, Adv. Colloid Interface Sci. 272 (2019) 102019, https://doi.org/10.1016/j.cis.2019.102019.

[30] J.S. Lee, Y.S. Choi, J.S. Lee, E.J. Jeon, S. An, M.S. Lee, H.S. Yang, S.W. Cho, Mechanically-reinforced and highly adhesive decellularized tissue-derived hydrogel for efficient tissue repair, Chem. Eng. J. 427 (2022) 130926, https://doi.org/10.1016/j.cej.2021.130926.

[31] L. Falcão, M.E.M. Araújo, Application of ATR–FTIR spectroscopy to the analysis of tannins in historic leathers: the case study of the upholstery from the 19th century

portuguese royal train, Vib. Spectrosc. 74 (2014) 98–103, https://doi.org/10.1016/j.vibspec.2014.08.001.
[32] C. Stani, L. Vaccari, E. Mitri, G. Birarda, FTIR investigation of the secondary structure of Type I collagen: new insight into the amide III band, Spectrochim. Acta. A. Mol. Biomol. Spectrosc. 229 (2020) 118006, https://doi.org/10.1016/j.saa.2019.118006.
[33] Z. Qin, Y. Huang, S. Xiao, H. Zhang, Y. Lu, K. Xu, Preparation and characterization of high mechanical strength chitosan/oxidized tannic acid composite film with schiff base and hydrogen bond crosslinking, Int. J. Mol. Sci. 23 (2022) 9284, https://doi.org/10.3390/ijms23169284.
[34] M. Božič, S. Gorgieva, V. Kokol, Homogeneous and Heterogeneous Methods for Laccase-Mediated Functionalization of Chitosan by Tannic Acid and Quercetin, Carbohydr. Polym. 89 (2012) 854–864, https://doi.org/10.1016/j.carbpol.2012.04.021.
[35] W. Kong, Q. Du, Y. Qu, C. Shao, C. Chen, J. Sun, C. Mao, R. Tang, X. Gu, Tannic acid induces dentin biomineralization by crosslinking and surface modification, RSC Adv. 12 (2022) 3454–3464, https://doi.org/10.1039/D1RA07887A.
[36] J. Zhao, F. Pan, P. Li, C. Zhao, Z. Jiang, P. Zhang, X. Cao, Fabrication of ultrathin membrane via layer-by-layer self-assembly driven by hydrophobic interaction towards high separation performance, ACS Appl. Mater. Interfaces 5 (2013) 13275–13283, https://doi.org/10.1021/am404268z.
[37] M.H. Iqbal, A. Schroder, H. Kerdjoudj, C. Njel, B. Senger, V. Ball, F. Meyer, F. Boulmedais, Effect of the buffer on the buildup and stability of tannic acid/collagen multilayer films applied as antibacterial coatings, ACS Appl. Mater. Interfaces 12 (2020) 22601–22612, https://doi.org/10.1021/acsami.0c04475.
[38] N. Sahiner, S. Sagbas, M. Sahiner, C. Silan, N. Aktas, M. Turk, Biocompatible and biodegradable Poly(Tannic Acid) hydrogel with antimicrobial and antioxidant properties, Int. J. Biol. Macromol. 82 (2016) 150–159, https://doi.org/10.1016/j.ijbiomac.2015.10.057.
[39] C.Y. Liu, M. Matsusaki, M. Akashi, Cell effects on the formation of collagen triple helix fibers inside collagen gels or on cell surfaces, Polym. J. 47 (2015) 391–399, https://doi.org/10.1038/pj.2015.2.
[40] K. Adamiak, A. Sionkowska, Current methods of collagen cross-linking: review, Int. J. Biol. Macromol. 161 (2020) 550–560, https://doi.org/10.1016/j.ijbiomac.2020.06.075.
[41] L. Aubert, M. Dubus, H. Rammal, C. Bour, C. Mongaret, C. Boulagnon-Rombi, R. Garnotel, C. Schneider, R. Rahouadj, C. Laurent, S.C. Gangloff, F. Velard, C. Mauprivez, H. Kerdjoudj, Collagen-based medical device as a stem cell carrier for regenerative medicine, Int. J. Mol. Sci. 18 (2017) 2210, https://doi.org/10.3390/ijms18102210.
[42] F. Reitzer, E. Berber, J. Halgand, V. Ball, F. Meyer, Use of gelatin as tannic acid carrier for its sustained local delivery, Pharm. Front. 2 (2020) e200002, https://doi.org/10.20900/pf20200002.
[43] W. Chariyarangsitham, S. Krungchanuchat, P. Khuemjun, C. Pilapong, Effect of advanced oxidation and amino acid addition on antioxidant capability, iron chelating property and anti-cancer activity of tannic acid, Arab. J. Chem. 14 (2021) 103312, https://doi.org/10.1016/j.arabjc.2021.103312.
[44] H. Cao, D. Xiang, X. Zhou, P. Yue, Y. Zou, Z. Zhong, Y. Ma, L. Wang, S. Wu, Q. Ye, High-strength, antibacterial, antioxidant, hemostatic, and biocompatible Chitin/PEGDE-tannic acid hydrogels for wound healing, Carbohydr. Polym. 307 (2023) 120609, https://doi.org/10.1016/j.carbpol.2023.120609.
[45] Y. Wang, H. Qi, Y. Liu, C. Duan, X. Liu, T. Xia, D. Chen, H.L. Piao, H.X. Liu, The double-edged roles of ROS in cancer prevention and therapy, Theranostics 11 (2021) 4839–4857, https://doi.org/10.7150/thno.56747.
[46] R. Kanoi, P. Loachan, S. Das, B.S.S. Rao, Mangiferin, a naturally occurring polyphenol, mitigates oxidative stress induced premature senescence in human dermal fibroblast cells, Mol. Biol. Rep. 48 (2021) 457–466, https://doi.org/10.1007/s11033-020-06074-2.
[47] J. Zhu, Y. Li, W. Xie, L. Yang, R. Li, Y. Wang, Q. Wan, X. Pei, J. Chen, J. Wang, Low-swelling adhesive hydrogel with rapid hemostasis and potent anti-inflammatory capability for full-thickness oral mucosal defect repair, ACS Appl. Mater. Interfaces 14 (2022) 53575–53592, https://doi.org/10.1021/acsami.2c18664.
[48] M.R. Villegas, A. Baeza, A. Usategui, P.L. Ortiz-Romero, J.L. Pablos, M. Vallet-Regí, Collagenase Nanocapsules: an approach to fibrosis treatment, Acta Biomater 74 (2018) 430–438, https://doi.org/10.1016/j.actbio.2018.05.007.
[49] J.K. Jackson, J. Zhao, W. Wong, H.M. Burt, The inhibition of collagenase induced degradation of collagen by the galloyl-containing polyphenols tannic acid, epigallocatechin gallate and epicatechin gallate, J. Mater. Sci. Mater. Med. 21 (2010) 1435–1443, https://doi.org/10.1007/s10856-010-4019-3.
[50] S.E. Moujahed, F. Errachidi, H.A. Oualid, A.V. Botezatu-Dediu, F.O. Chahdi, Y. K. Rodi, R.Mihaela Dinica, Extraction of insoluble fibrous collagen for characterization and crosslinking with phenolic compounds from pomegranate byproducts for leather tanning applications, RSC Adv 12 (2022) 4175–4186, https://doi.org/10.1039/D1RA08059H.
[51] J. Zhang, W. Wang, Z. Pei, J. Wu, R. Yu, Y. Zhang, L. Sun, Y. Gao, Mutagenicity assessment to pesticide adjuvants of toluene, chloroform, and trichloroethylene by ames test, Int. J. Environ. Res. Public. Health 18 (2021) 8095, https://doi.org/10.3390/ijerph18158095.
[52] M. Jurak, A.E. Wiącek, A. Ładniak, K. Przykaza, K. Szafran, What affects the biocompatibility of polymers? Adv. Colloid Interface Sci. 294 (2021) 102451 https://doi.org/10.1016/j.cis.2021.102451.
[53] M. He, X. Gao, Y. Fan, L. Xie, M. Yang, W. Tian, Tannic Acid/Mg2+-based versatile coating to manipulate the osteoimmunomodulation of implants, J. Mater. Chem. B 9 (2021) 1096–1106, https://doi.org/10.1039/D0TB01577F.
[54] A.E. Hanselman, J.E. Tidwell, R.D. Santrock, Cryopreserved human amniotic membrane injection for plantar fasciitis: a randomized, controlled, double-blind pilot study, Foot Ankle Int 36 (2015) 151–158, https://doi.org/10.1177/1071100714552824.
[55] H. Rammal, L. Entz, M. Dubus, A. Moniot, N.B. Bercu, J. Sergheraert, S.C. Gangloff, C. Mauprivez, H. Kerdjoudj, Osteoinductive material to fine-tune paracrine crosstalk of mesenchymal stem cells with endothelial cells and osteoblasts, Front. Bioeng. Biotechnol. 7 (2019) 256, https://doi.org/10.3389/fbioe.2019.00256.
[56] N. Xu, Y. Gao, Z. Li, Y. Chen, M. Liu, J. Jia, R. Zeng, G. Luo, J. Li, Y. Yu, Immunoregulatory hydrogel decorated with tannic acid/ferric ion accelerates diabetic wound healing via regulating macrophage polarization, Chem. Eng. J 466 (2023) 143173, https://doi.org/10.1016/j.cej.2023.143173.